Classical and Quantum Gravity

PAPER

OPEN ACCESS

RECEIVED
31 October 2025

REVISED
9 February 2026

ACCEPTED FOR PUBLICATION
31 March 2026

PUBLISHED
16 April 2026

Enhancing the scientific exploitation of future gravitational wave experiments through a multi-messenger approach

Florentina-Crenguta Pislan[1,2,*], **Laurentiu-Ioan Caramete**[1] **and Ana Caramete**[1,*]

[1] Institute of Space Science—INFLPR Subsidiary, 409 Atomistilor, Magurele, Romania
[2] Doctoral School of Physics, Faculty of Physics, University of Bucharest, 405 Atomistilor, Magurele, Romania
[*] Authors to whom any correspondence should be addressed.

E-mail: fcpislan@spacescience.ro and acaramete@spacescience.ro

Keywords: gravitational waves, multi-messanger astronomy, source catalogs, astrophysics

Abstract

We propose a multi-messenger approach by using electromagnetically observed parameters, like masses and redshifts, to refine predictions on the gravitational wave (GW) detection, while exploring unknown parameters, such as spins. This approach aims to construct a comprehensive observational catalog consisting of potential GW sources such as mergers of supermassive black holes (BHs) in quasars and *X*-shaped radio galaxies. Through a literature review, we compiled a preliminary catalog of potential sources. For these identified systems, we determined the key parameters crucial for GW modeling. One of our goals with this is to create a library of potential gravitational waveforms that could serve the GW community as training/testing data for the data analysis pipelines. This database is also meant to be used for the development of future data analysis tools that will be essential in processing and interpreting the data produced by the current and upcoming GW experiments. Using the LISA data challenge tools, so far we have modeled over 20 000 gravitational waveforms coming from potential systems of massive BH binaries and we intend to extend it up to a few hundred thousand waveforms coming from other binary systems as well. In this paper, we present the methods used for estimating the parameters of those sources that could emit electromagnetic counterparts of the GWs that LISA and other next-generation GW experiments may detect.

1. Introduction

With the recent adoption of the LISA (Laser Interferometer Space Antenna) Space Mission, new opportunities emerge in the field of GW research, and the need for an extended source database is even greater because we need to be ready for any potential scenario the LISA constellation may encounter. Despite the fact that almost a decade has passed since the first GW was detected, we still do not have enough case studies for what future experiments may uncover, making it difficult to anticipate the full range of scenarios detectable by these upcoming GW experiments. LISA is best known as the largest space mission designed to detect GWs in the frequency range of 10^{-5}–10^{-1} Hz, and is particularly sensitive to signals coming from massive black hole binary systems (MBHBs), with component masses between 10^3–$10^7\,M_\odot$, as well as other compact binary systems.

Despite already considering these main sources for LISA, one can never be too prepared. The possibility that LISA could detect GWs coming from more exotic or unforseen GW sources—such as events involving star gulping phenomena [9] or extreme mass ratio inspirals (EMRIs)—is not excluded. So, in order to ease the process of identifying such potential new sources, we started developing a library of simulated gravitational waveforms so that the parameters of the sources could be traced back more easily. The waveform library is based on a curated database of candidate binary sources identified in the literature, which are likely to be detectable by LISA. For each candidate, we extended the existing information with data from astronomical observational catalogs, allowing us to complete our collection of sources with updated or estimated source parameters. Despite extensive analysis, the sources

considered in this study remain only partially characterized, necessitating the constraint of several key physical parameters. The most important parameter to be constrained was the mass of each object; the estimation methods we used for this will be further discussed in section 2.1.

In this paper, we adopt a multi-messenger approach for better constraining the origin and properties of the considered binary systems by combining electromagnetic observations with GW simulations. In this way, we improve our ability to evaluate whether known electromagnetic sources could emit GWs detectable by LISA.

One of the sources that has piqued our curiosity for this specific study is one that has been on astronomers' radar ever since 1974, when its unique morphology was for the first time described in [23]. These particular sources—which we will from now on refer to as *X*-shaped radio galaxies (XRGs) - are a distinct type of extragalactic radio source, that are typically massive, early-type elliptical galaxies that host an active nucleus ejecting relativistic plasma jets. XRGs are defined by two misaligned pairs of radio lobes emanating from the same host galaxy, creating their distinctive *X*-shaped structure. These pairs of lobes can be characterized as primary lobes and secondary or 'winged' lobes, the latter being less collimated than the primary ones.

Based on the potential formation scenarios which are presented in detail in [19], XRGs may trace back to supermassive black hole (SMBH) mergers, with their morphology serving as evidence of a recent coalescence. Such mergers are predicted to be strong sources of GWs ([15, 45]), particularly detectable in the LISA band for lower-mass SMBHs.

A key set of parameters for binary black holes (BHs) is the spin of the components and their evolution. In the spin-flip model, the spin of the dominant SMBH can realign during the late stages of the binary evolution and/or after coalescence, leading to an abrupt change in the jet direction and strong gravitational-wave emission [39]. In this picture, the X-shaped radio morphology is interpreted as a consequence of a spin flip of the dominant black hole. In this framework and within the one-dominant-spin approximation in which the secondary spin is neglected, the total angular momentum of the binary is written as $J \simeq L + S_1$, where L is the orbital angular momentum and S_1 is the dominant black hole spin (i.e. the spin of the more massive black hole). As the binary inspirals and the separation decreases, gravitational-wave emission removes orbital angular momentum, so the magnitude of L decreases while S_1 remains approximately constant. The system therefore evolves from an orbit-dominated regime, $L \gg S_1$ to a spin-dominated regime $S_1 \gg L$. Moreover, let α denote the angle between the orbital angular momentum L and the total angular momentum J, and let β denote the angle between the dominant black hole spin S_1 and J. Since the orbital angular momentum decreases during the inspiral because of gravitational-wave emission, α increases with time, meaning that L progressively tilts away from J. At the same time, β decreases, so the spin of the dominant black hole becomes progressively more aligned with the total angular momentum. Thus, as the binary evolves and the orbital angular momentum decays, the spin of the dominant black hole becomes the principal contribution to J. In the spin-flip scenario, this can lead to a reorientation of the jet axis and potentially to observable electromagnetic signatures.

Spin-flip is significant in the ranges of mass ratios for which the ratio S/L changes from less than 1 to greater than 1 during inspiral.

The constancy of the total angular momentum direction leads to a change in the spin direction, which makes this particular type of sources such an interesting case study for the parameter of spin of GW sources. During the final inspiral, the decaying orbital momentum can induce rapid jet precession; if these relativistic jets align near our line of sight, they may produce strong multi-wavelength variability: an electromagnetic precursor occurring years before coalescence [19].

Moreover, the model links GW emission to specific electromagnetic signatures [17]. Detecting such correlations would provide compelling evidence for the role of SMBH mergers in powering active galactic nuclei (AGNs). The second spin-flip stage, marked by rapid precession, is predicted to proceed about 10^4 times faster than the first, lasting only a few years, making it an observationally accessible timescale. The main channel of observation in this case would be primarily electromagnetically, as the new jets will drive a new path in the interstellar medium, they could encounter zones of various density that can create shock processes, when the flow can go supersonic. This can accelerate particles to very high energies and also create EM signatures. We plan to further investigate such cases in the future and to study how and when the spin-flip can occur in a special multi-messenger article connecting the GW signal with observation in radio.

All these arguments point out to XRGs as being a great source to analyze from the perspective of studying both the spin-flip scenario and the GW emission.

Besides, considering the electromagnetic signature, XRGs represent the perfect case study for our multi-messanger approach of developing an observational catalog of binary sources. After developing

a catalog of sources with their parameters, we also consider modeling the potential gravitational waveforms that might be emitted by the XRGs. For this, we use dedicated tools developed by the LISA data challenge (LDC) Group [4]. Each simulation uses a set of 15 parameters, including both intrinsic parameters (such as masses and spins) and extrinsic ones (such as redshift and coordinates in the sky). For candidate sources with binary behavior, we modeled the unknown parameters to generate plausible GW signals.

This approach could be successfully used to constrain source parameters and improve our understanding of binary systems.

2. Catalog of binary sources

In this section, we present the catalog of XRGs that we had put together based on observations from literature. Our specific contribution to it consists in the estimation of those specific parameters needed for simulating the corresponding GWs. For one simulation, we need a set of 15 parameters of the sources consisting in: masses, spins, ecliptic coordinates, redshift, luminosity distance, inclination, polar and azimuthal angles of spins, phase, observation duration and time to coalescence. Of all of these, we are particularly interested in estimating the masses and spins, as they are considered to be sufficient for the characterization of an inspiralling compact binary model [5], which also explains the strong influence of the intrinsic parameters on a gravitational waveform compared to the one exerted by the extrinsic ones. For the rest, we either already have the information from the electromagnetic observations, or we are able to generate as many potential parameter combinations as computationally possible in order to cover all possible scenarios. The method used for estimating each of the parameters is further detailed in the next subsections.

For this analysis, we consider two different sets of XRGs gathered from the observational literature:

1. the confirmed *X*-shaped objects from [40] which had the total mass of the binary system already observed, as well as known redshift and coordinates;
2. potential *X*-shaped objects for which the only known parameters useful for the simulation are the coordinates and the redshift.

For these systems, parameter estimation was carried out with the goal of obtaining suitable values to use in GW simulations. Accordingly, for each selected sample, we began by estimating the masses of the individual objects in the binary system.

2.1. Parameter estimation

As already mentioned in the previous section, the source samples used for this study were gathered from the observational literature, thus part of the parameters were already known, while others had to be estimated.

For each case, we used a different approach for estimating the masses. It is well known that the influence of the component masses of a BH binary (BHB) system on the resulting gravitational waveform is dependent on the mass ratio of the two compact objects. Thus, considering m_1 and m_2 the masses of the two BHs, the mass ratio q can be expressed as:

$$q = \frac{m_1}{m_2}, m_1 \geqslant m_2. \tag{1}$$

According to [18], the SMBH spin-flip effect during the inspiral stage could explain the observations made on the XRGs. Since we analyze the same type of sources as in [18], it is only natural to use the same mass ratio ranges, together with the finding that they have approximately the same probability:

- $q_1 \in (1, 1/3)$;
- $q_2 \in (1/3, 1/10)$;
- $q_3 \in (1/10, 1/30)$;
- $q_4 \in (1/30, 1/100)$;
- $q_5 \in (1/100, 1/300)$;
- $q_6 \in (1/300, 1/1000)$.

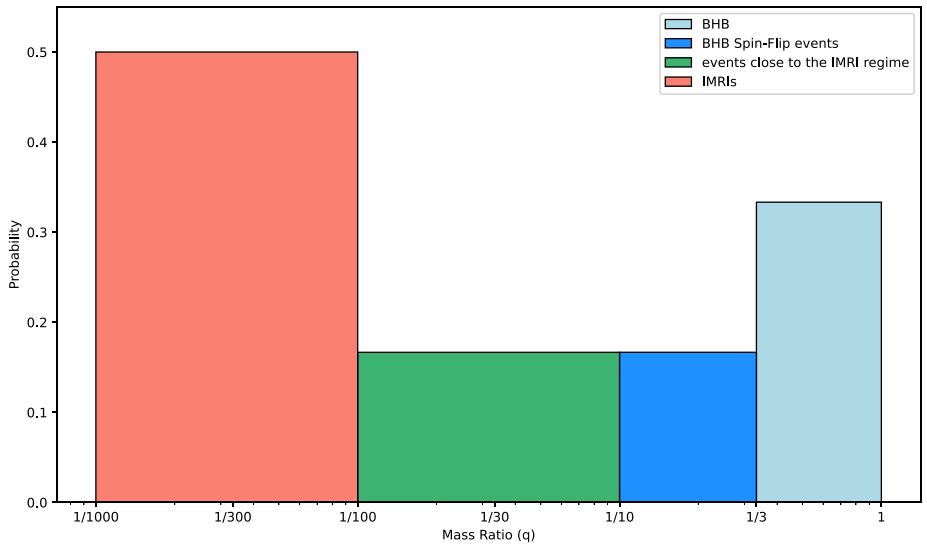

Figure 1. Bar plot presenting the probability for different types of astrophysical events to happen based on the mass ratio of the sources from each XRG system.

We estimate the merger rates associated with different types of binary systems, as well as the masses of each individual object forming a binary. We detail this analysis in sections 2.1.1 and 2.1.2.

2.1.1. Method 1

For the first approach, we considered the population of 29 XRGs that had already been observed and confirmed in [40], together with a control sample of 36 additional objects. Although the population considered is fairly low to estimate an accurate mass function from it, the available parameters for these sources allowed us to consider the scenarios described in [18]. This means that we had at our disposal the total mass of the systems (M), which was inferred from the stellar velocity dispersion according to [2], and which can also be expressed as:

$$M = m_1 + m_2 \Rightarrow m_1 = \frac{M}{1+q}, \tag{2}$$

where the potential mass ratios (q) between any two BHs forming one binary system is expressed as shown in equation (1), and the probability (p) that each mass ratio scenario could occur.

We also incorporated the errors given in [40], where the total BH mass of the system is obtained from the stellar velocity dispersion, σ_*, and which computes the mass on the premise that the dynamics of the host galaxy's stellar bulge is controlled by the gravitational influence of the central SMBH:

$$M = 1.349 \times 10^8 M_\odot \left(\frac{\sigma_*}{200\,\mathrm{kms}^{-1}}\right)^{4.02\pm0.32}. \tag{3}$$

When solving the equation system corresponding to this particular set of galaxies, we got 29×10^5 potential combinations of the solutions m_1 and m_2, which were obtained with respect to the logarithmically even distributions. That means that we had to be careful to have the same number of values in each q interval, N. We obtained this by applying the step size formula:

$$s = \frac{x_{\max} - x_{\min}}{N-1} \tag{4}$$

where s is the step, and $x_{\max}$ and $x_{\min}$ represent the maximum and the minimum values from each of the considered intervals.

By analyzing the distribution of the obtained mass ratios, we found the event rates for BHBs, BHBs in the spin-flip scenario, events happening close to the intermediate mass ratio inspirals (IMRIs) and IMRIs. For this, we considered the astrophysical constraints presented in [1] as follows: $1 \leqslant q_{\mathrm{BHB}} \leqslant 1/10$ for BHBs, $10^{-5} \leqslant q_{\mathrm{IMRI}} \leqslant 10^{-2}$ for IMRIs, and $q \lesssim 0.01$ for those events happening close to the IMRI regime. As can be seen in figure 1, the highest probability was obtained for IMRI events, being about 50%. The other half of the events is roughly equally distributed between the other types of considered

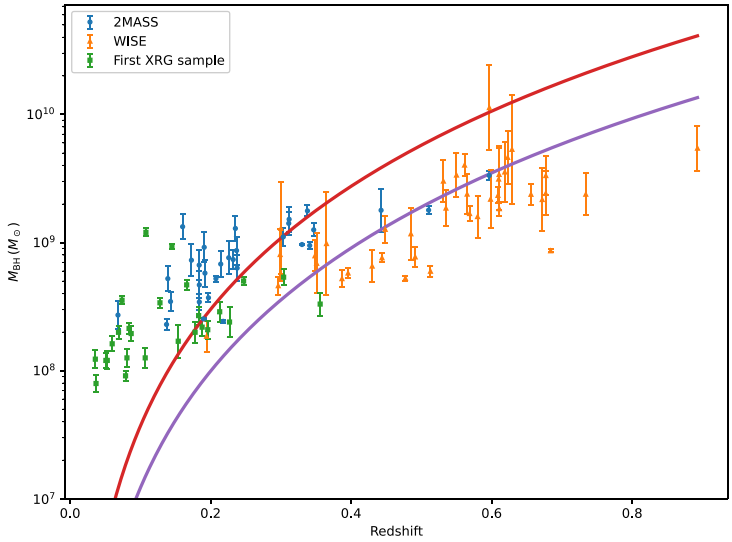

Figure 2. The total estimated mass in logarithmic scale for each source from the entire XRG sample considered as a function of redshift. The first sample consists in objects already identified as XRGs [40], here represented in green, while the blue and orange data points represent the second sample of XRGs from appendix, for which the masses were estimated with respect to the flux density extracted from 2MASS (blue) and WISE (orange) catalogs. The masses extracted from the 2MASS catalog are presented in table 3 and the masses extracted from the WISE catalog are presented in table 4. Please note that tables 3 and 4 contain the logarithmic values of $M_{\rm BH}(M_\odot)$, while the Y axis in figure 2 shows the actual mass values. The selection curves for elliptical galaxies are represented in red for the XRG sample with the flux extracted from 2MASS catalog, and in purple for the XRG sample with the flux extracted from WISE catalog.

events as follows: 16.67% probability for events close to the IMRI regime to happen, while the other third of the events are represented by BHB events out of which half of them have the potential of presenting the spin-flip phenomenon, while the rest are 'simple' BHB events.

2.1.2. Method 2

In this part of the study, we worked with different kinds of data, which led to the need to find a different approach. This sample consists of sources mainly labeled as 'potential candidates' for XRGs, and therefore, as potential binary systems capable of generating GWs. Unlike the first sample, the second sample consists in systems whose masses were not previously determined. For this reason, we had to start by estimating the total mass of each system, and only then would we look for all the potential combinations of masses for the two objects, similar to what we did in the first method.

To estimate the total mass of the considered systems, we started by analyzing the data collected in NED for each of these sources. We extracted information on redshift, ecliptic coordinates and the flux density. The redshift for the considered XRGs is in the range $[0.68; 0.893]$. For finding the proper way to estimate the masses, we also took into consideration the outputs of different BH simulation codes which are based on semi-analytical methods (SAMs) and hydrodynamical simulations. We examined models whose redshift coverage includes that of the XRG sample, specifically: L-galaxies [22, 26, 27], BACH, NewHorizon [44], KETJU simulations [37], Illustris [41], SIMBA, Horizon-AGN [44], EAGLE [14], MassiveBlackII [34], BlueTides [16], SHARK [36], Astraeus, A-SLOTH [20, 21], GQD. The BH mass functions obtained from the SAMs and hydridynamical simulations match in results at $z \in (0, 1)$ because that is where most observational information exists [32, 46]. Given this and the XRG redshift range, we extrapolated the BH mass function developed for BHs in the local Universe [8] to our sample.

The BH mass function can be written as a relation of proportionality between the density flux from the 2MASS catalog, $f_{2\mu}$, and the luminosity distance, D [8].

To go from a proportionality relation to an equality relation, we will use the correction factor R obtained for the 2 micron emission in [10] and a scaling factor of 10^6. [7, 19] state that XRGs occur only in elongated elliptical hosts (ellipticity ≈ 0.2), with observations indicating clear links between radio structure and optical morphology, so we chose the R factor accordingly. The values for the 2 micron density flux in IR for our samples were taken from the 2MASS and WISE catalogs, depending on the source.

Our initial sample of potential XRGs consisted in 108 systems. However, not all of them present information on the flux density, so our final sample only consisted in 70 sources.

Table 1. Frequncy of the last stable circular orbit in the detector-frame, time spent by the signal in the LISA band and SNR for the sources at the LISA limit, with masses expressed in the source-frame.

$\log M\,(M_\odot)$	$f_{\rm ISCO}$ (mHz)	Time in band (days)	SNR range
7.05 ± 0.45	0.2812	2.6802	(633.79; 53 757.94)
7.65 ± 0.05	0.0791	0.2581	(899.46; 864 152.41)
7.68 ± 0.23	0.0604	0.2459	(187.71; 24 699.72)

After estimating the total mass for our new sample, we also estimate the component mass values m_1 and m_2 for each of the objects of the binary systems considered in this second scenario. For this, we followed the same method as for the first XRG sample.

The total masses derived from applying this mass function to our samples are presented in appendix. These, along with the rest of the electromagnetically observed parameters, are stored in the GW Repository.

The observational limits for a sample of elliptical galaxies can be defined with the help of a selection curve which can give us the smallest BH mass that can be detected for a given redshift and flux limit. And so, for each of the surveys used for extracting the flux values for our mass estimation analysis, we computed an apparent magnitude based on the observed flux and the zero-point flux. For the 2MASS survey, we considered the zero-point flux as being $666.7Jy$ [12], while for the WISE survey, we considered the value 309.54 Jy [28]. Then, we calculated the absolute magnitude using the distance and the solar absolute magnitudes in the bands K_s for the values from the 2MASS survey, and $W1$ or those from the WISE survey. We can now express the luminosities which will be useful in getting the mass-to-light ratios. Considering that we are analyzing elliptical galaxies, we can assume a constant mass-to-light ratio for estimating the the stellar mass [6, 25]. The elliptic galaxies are bulge dominated [35], so we can roughly approximate the stellar mass with the bulge mass, thus getting to have a BH mass-bulge relation for which the considered fit parameters are the ones from [38]: $\alpha = 8.54 \pm 0.15$ and $\beta = 1.11 \pm 0.28$. We used the same two fit parameters for fitting the data points from the two surveys; however the curves do not overlap because they are computed based on the minimum estimated BH mass for the given redshift, which is different for each surveys.

2.2. Detectability in LISA

LISA is designed to detect GWs in the millihertz (mHz) frequency band, specifically between 10^{-4}Hz and 10^{-1}Hz, with peak sensitivity around a few mHz. MBHBs fall within this frequency range, emitting GWs during their late inspiral, merger, and ringdown phases [13]. The exact frequency at which MBHBs enter the LISA band depends on their mass and redshift.

In the catalog we developed, we present multiple cases of BHB systems, with total masses ranging from $10^7 M_\odot$ to $10^9 M_\odot$. And so, our catalog is suitable for studying both limit LISA cases (for those sources having a total mass of $10^7 M_\odot$ and which would barely enter the lower region of the LISA band), and systems visible for other GW detectors, such as GUEST (Gravitational Universe Exploration with Satellite Tracking) (call page). For those extreme LISA cases presented in our catalog, we are expecting signals that might have the frequencies ranging from about 0.06 mHz to around 0.28 mHz, and which would remain detectable in the LISA band for approximately 6 hours to a bit over 2 days. These calculations were made according to [42] and the results are explicitly presented in table 1.

Previous work ([2, 3, 29–31, 42]) showed that MBHB systems with a total mass between 10^5–$10^7 M_\odot$ can reach signal-to-noise ratios (SNRs) of order 100–1000 s, which would mean that LISA would have great performances in estimating parameters like masses, spins, redshift and sky localization. We found that the SNRs of the MBHB sources from our catalog range between 187 to 86 452, which are values validated by previous work and so that might fit the LISA sensitivity band.

However, we stress that although we have only considered those science cases that correspond to the currently required minimum frequency ($0.1\ mHz$), we do not exclude the possibility that additional sources from our catalog may also be visible by LISA if the performance demonstrated by LISA Pathfinder (featuring a bandwidth extending down to $20\ \mu Hz$ [13]) is confirmed. In such a scenario, the SNR computation method would differ from the one adopted for what we currently present as cases as the detection treshold, as higher harmonics would need to be considered in the calculation [42].

Table 2. Parameter range values injected in the simulation code for producing the GW templates. The masses are the ones estimated according to the methods described in section 2.1, the redshift values is the one labeled in tables 3 and 4. For each redshift, we computed the luminosity distance by considering the ΛCDM model, for which the Hubble costant is $H_0 = 67.1$, and the dark energy density parameter is $\Omega_0 = 0.3175$. We consider the observation duration to be one year, which is the time needed for the LISA constellation to complete one rotation around the Sun.

Parameter name	Value range
Ecliptic latitude	$(\pi/2; +\pi/2)$ rad
Ecliptic longitude	$(0; 2\pi)$ rad
Polar angles of spins	$(0; \pi)$ rad
Phase at coalescence	$(0; 2\pi)$ rad
Initial polar angle	$(0; \pi)$ rad
Initial azimuthal angle	$(0; 2\pi)$ rad

3. Database of gravitational waveforms

In addition to the catalog of binary sources, we also started developing a library of gravitational waveforms, simulated based on the estimated parameters. The waveforms are of the 'template' type, meaning temporal representations of the plus and cross polarizations. Thus, they can be passed through the instrument in a way characteristic of each GW experiment. The need for such a database originates in the relatively small number of GW detections, as well as in the lack of real study cases of GW source parameters. For instance, for the development of a low-latency alert pipeline that would emit fast alerts to other observatories as soon as LISA detects a GW signal, realistic data are of great help for easing the process of parameter estimation in the purpose of localizing on sky the astrophysical event.

Our GW database can also serve as an useful resource for the future generation of GW experiments, such as GUEST, in their effort of detecting GWs coming from SMBHBs with masses ranging from $10^6 M_\odot$ to $10^9 M_\odot$. This mission aims to detect GWs in the nHz–μHz frequency band, as well as to identify the individual SMBHs and EMRIs that generated them. Therefore, using an already existing catalogue of potential SMBHB sources would facilitate the search for these systems and support mission preparation. For more information on the mission proposal call where GUEST was accepted, go to the call page.

To calculate the 'generic time-domain instrument response to GWs', we used the LISA GW Response code [4], developed in the LISA Collaboration. The source code is publicly available at this GitLab Repository. The cosmological model adopted in the simulations is (Flat)LambdaCDM, and the approximant used is IMRPhenomD.

The IMRPhenomD approximate model was specially designed to model GWs from the merger of BHBs. This specific kind of GW has three different stages (inspiral, merger and ringdown) with three different theoretical approaches (Post-Newtonian theory, numerical relativity, perturbation theory), which is why the approximant uses distinctive formulas for computing the effective spin according to the analyzed stage [24, 33, 43]. The amplitude and phase terms are also computed according to the waveform stage and, in the end, all of these terms are used for the construction of the final phase and amplitude functions.

The simulation code uses a total of 15 parameters belonging to either one of the two objects forming the binary source, or to the binary system itself. The set is composed of both intrinsic (masses and spins) and extrinsic parameters (coordinates, redshift, luminosity distance).

The samples considered for this study have part of the needed parameters (such as redshifts, or even coordinates for some of the sources) already known. For the rest of the parameters needed for one simulation, we had to find specific methods to estimate each of them. The masses were estimated according to the methods described in section 2.1, and the redshift values are the ones from the considered catalogs.Other than the masses, spins and redshift, all the other parameters could easily be estimated as being uniformly distributed within certain limits considering the astrophysical and cosmological constrains imposed by the type of source. The range of values for each of these parameters is described in table 2. The same approach was used for the Sangria LDC database, so we considered this method to be already verified and with a certain background.

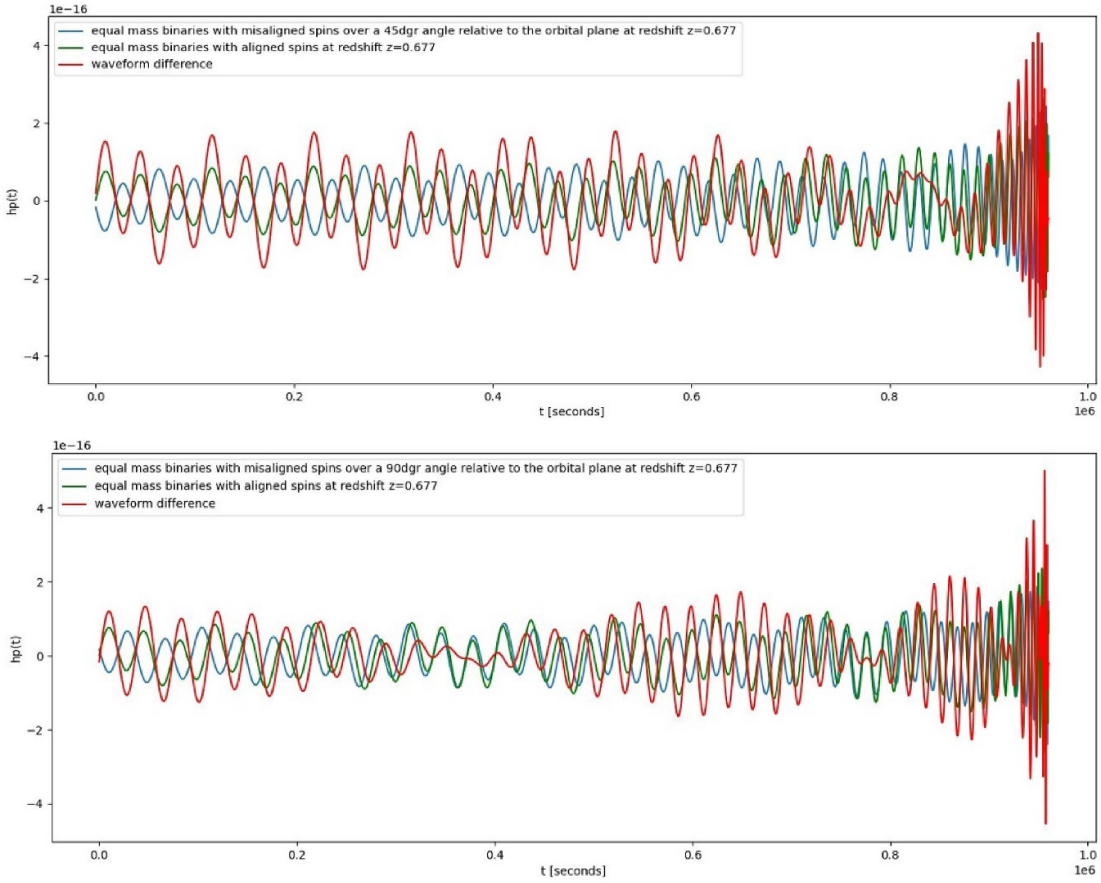

Figure 3. Comparison in waveform (red) between the GWs emitted by an equal mass binary when the spins of the black holes are aligned (green) opposed to the case of misaligned spins (blue). In the upper plot, is presented the case of a 45 degree tilt leading to the misalignment of spins, while the lower plot presents a spin misalignment scenario given by a 90 degree tilt.

For each of the mass estimates, we generated potential values for the rest of the parameters to be injected into a waveform simulation. Each such set of combined parameters was included in the simulation code for producing time series of the plus and cross polarizations that a GW coming from a source with those specific parameters could have. In this way, we put together a library of potential GW templates. These represent the clean signal coming from the sources, which can then be injected through the experiment simulator for which an analysis is made.

As a concrete example of what the templates look like, we present figure 3 in which is represented the plus polarization as a function of time for a signal coming from an equal mass binary source at the LISA limit, and with a known redshift ($z = 0.677$).

In order to emphasis the effect of misaligned spins, for this example, we intentionally chose to overlap in figure 3 the 2 possible templates: one corresponding to the configuration in which the two spins are aligned (represented with the green line in figure 3), and the one in which the two spins are misaligned by an angle of $\pi/2$ (represented with the blue line in figure 3). The waveform difference of the two is represented in red.

Although the approximant that we used in the simulation does not have explicit precession, we simulated this process for the inspiral phase by manually changing the polar angles of the spins so that they would be the same for the alligned scenario, or different with a $\pi/2$ angle for the misalligned scenario, while keeping all the other parameters fixed. In this way, we could get a qualitative idea of what the spin-flip effect might be like. The next natural step in our analysis is to get a more accurate waveform by using approximants with precession, such as IMRPhenomPv2/Pv3 [11].

All waveforms simulated for this study are available in our public GW Repository.

4. Conclusions

The study presented here highlights the preparatory work required for the upcoming LISA mission and other future GW experiments or missions, focusing on building an extended and versatile database of potential GW sources. By combining multi-messenger observations, linking electromagnetic and gravitational data, the research provides a framework for identifying, modelling, and understanding sources that LISA may detect.

Among the various classes of sources, XRGs emerge as particularly valuable targets. Their unique morphology and the potential link to SMBH mergers make them excellent case studies for investigating spin-flip phenomena and jet realignment processes associated with GW emission. The analysis demonstrates that XRGs not only trace the aftermath of SMBH mergers but also may serve as electromagnetic counterparts of GW events.

Using the IMRPhenomD approximant, a library of gravitational template waveforms was generated to represent signals from XRG-like binary systems. This waveform database will play a key role in testing and calibrating GW detector data analysis pipelines, improving the detection and characterization of future GW sources.

This work represents an important step toward bridging electromagnetic and gravitational observations and establishing a catalog of potential GW sources. The results confirm that XRGs are not only interesting astrophysical objects but also promising laboratories for studying GW emission.

In our future work, we will focus on expanding the catalogue to include a wider range of potential sources and implementing additional waveform approximants in the simulation code. This will aid the generation of increasingly accurate waveforms, further enhancing our ability to characterize and detect diverse GW signals with LISA and other future generation GW experiments.

Acknowledgments

This work is supported by the Romanian Ministry of Research, Innovation and Digitalization under the Romanian National Core Program LAPLAS VII—Contract No. 30 N/2023 and by ESA PRODEX project RoLISASpace.

This research has made use of the NASA/IPAC Extragalactic Database (NED), which is operated by the Jet Propulsion Laboratory, California Institute of Technology, under contract with the National Aeronautics and Space Administration.

Data availability statement

All data that support the findings of this study are included within the article (and any supplementary files).

Appendix. Estimated masses for the second XRG sample

In this section, only the estimated total masses and redshift values are labeled, while the rest of the parameters needed for simulating the corresponding gravitational waveforms are presented in our public GW Repository.

Table 3. Black hole masses with errors for the second XRG sample, with the flux density in 2MASS catalog.

Object Name	Redshift	$\log M(M_{\odot})$
4 C +12.02	0.143 000	8.75 ± 0.08
WISEA J012101.23+005 100.5	0.237 866	9.02 ± 0.10
WISEA J021635.79+024 400.8	0.184 000	8.89 ± 0.10
WISEA J072737.50+395 655.7	0.311 816	9.40 ± 0.09
B2 0812+38	0.172 747	9.09 ± 0.12
WISEA J081841.57+150 833.5	0.330 140	9.19 ± 0.00
WISEA J082400.50+031 749.6	0.214 458	9.05 ± 0.10
WISEA J084509.67+574 035.8	0.236 960	9.16 ± 0.11
WISEA J085942.67+585 116.8	0.442 700	9.49 ± 0.16
B3 0920+408	0.160 227	9.34 ± 0.10
WISEA J093238.29+161 157.4	0.190 951	9.19 ± 0.12
WISEA J094953.64+445 655.6	0.190 000	8.61 ± 0.01
WISEA J095640.77-000 123.7	0.139 170	8.94 ± 0.10
WISEA J101028.09+530 313.1	0.341 101	9.18 ± 0.03
WISEA J101732.47+632 954.0	0.183 827	9.05 ± 0.12
WISEA J104632.42-011 338.3	0.184 000	8.75 ± 0.06
WISEA J112848.70+171 104.7	0.346 797	9.31 ± 0.05
WISEA J113816.62+495 025.0	0.510 338	9.46 ± 0.03
MCG +03-30-100	0.068 222	8.65 ± 0.11
WISEA J125721.88+122 820.6	0.207 626	8.93 ± 0.02
WISEA J132404.20+433 407.1	0.337 892	9.46 ± 0.04
WISEA J134051.21+374 911.7	0.218 000	8.59 ± 0.01
WISEA J134002.91+503 539.6	0.232 221	9.08 ± 0.07
WISEA J140742.18+272 158.5	0.235 305	9.33 ± 0.09
HB89 1435+355	0.596 596	9.73 ± 0.03
WISEA J150904.13+212 415.2	0.311 275	9.37 ± 0.09
2MASX J16080917+2945 133	0.225 860	9.11 ± 0.13
B2 1646+26	0.137 339	8.57 ± 0.05
WISEA J202855.27+003 512.5	0.192 000	8.98 ± 0.10
WISEA J223628.91+042 751.9	0.303 535	9.26 ± 0.07
WISEA J233259.27+024 715.3	0.197 000	8.78 ± 0.03

Table 4. Black hole masses with errors for the second XRG sample, with the flux density in WISE catalog.

Object Name	Redshift	$\log M(M_{\odot})$
WISEA J003023.88+112 112.9	0.448 570	9.32 ± 0.10
B3 0716+407	0.387 000	8.93 ± 0.06
B2 0749+33	0.299 000	9.16 ± 0.19
WISEA J080006.87+495 755.0	0.395 700	8.97 ± 0.04
WISEA J081404.54+060 238.2	0.561 491	9.82 ± 0.09
WISEA J085236.11+262 013.4	0.477 306	8.93 ± 0.02
WISEA J085915.14+080 539.4	0.565 156	9.61 ± 0.15
WISEA J092346.38+361 407.3	0.734 000	9.61 ± 0.16
WISEA J100408.96+350 623.7	0.610 607	9.79 ± 0.21
4 C +05.43	0.672 000	9.61 ± 0.22
WISEA J103358.55+353 007.2	0.611 000	9.47 ± 0.05
WISEA J103900.82+354 050.5	0.568 617	9.44 ± 0.06
WISEA J103924.91+464 811.6	0.531 345	9.72 ± 0.16
B3 1051+473	0.430 000	9.04 ± 0.12
WISEA J113649.97+015 121.2	0.485 100	9.32 ± 0.19
WISEA J115225.56+201 602.1	0.444 000	9.09 ± 0.03
B3 1152+445	0.550 000	9.77 ± 0.17
PKS 1200-033	0.351 000	9.10 ± 0.21
WISEA J122550.46+163 343.3	0.656 014	9.59 ± 0.08
WISEA J125900.79+203 248.5	0.580 000	9.44 ± 0.16
WISEA J130854.25+225 822.3	0.677 168	9.76 ± 0.15
WISEA J131331.39+075 802.6	0.365 000	9.36 ± 0.32
4 C +41.25	0.296 300	8.88 ± 0.07
WISEA J132713.87+285 318.2	0.300 000	9.45 ± 0.29
WISEA J133051.06+024 843.1	0.622 826	9.92 ± 0.19
WISEA J134353.97+193 333.9	0.513 000	8.99 ± 0.04
WISEA J135518.06+094 023.5	0.618 700	9.82 ± 0.22
WISEA J140349.81+495 305.4	0.491 248	9.10 ± 0.08
WISEA J141702.13+201 903.3	0.535 000	9.50 ± 0.14
WISEA J142646.37+271 223.7	0.677 000	9.62 ± 0.16
WISEA J144547.32-013 045.7	0.610 000	9.77 ± 0.22
WISEA J150636.50+074 018.3	0.684 000	9.14 ± 0.01
WISEA J151149.33+045 536.2	0.893 000	9.98 ± 0.17
WISEA J151704.60+212 241.9	0.348 500	9.12 ± 0.12
WISEA J154413.17+161 929.6	0.598 433	9.60 ± 0.21
WISEA J154842.59+014 919.7	0.609 000	9.58 ± 0.06
WISEA J155416.03+381 132.6	0.194 242	8.49 ± 0.12
WISEA J162245.42+070 714.5	0.596 800	10.37 ± -0.28
WISEA J222802.35-065 355.1	0.629 000	10.12 ± 0.33

ORCID iDs

Florentina-Crenguta Pislan 0000-0002-0678-8148
Laurentiu-Ioan Caramete 0000-0002-3571-3145
Ana Caramete 0000-0002-8997-5730

References

[1] Amaro-Seoane P *et al* 2023 Astrophysics with the laser interferometer space antenna *Living Rev. Relativ.* **26** 2
[2] Amaro-Seoane P *et al* 2012 Low-frequency gravitational-wave science with eLISA/NGO *Class. Quantum Grav.* **29** 124016
[3] Amaro-Seoane P *et al* 2012 eLISA: astrophysics and cosmology in the millihertz regime
[4] Baghi Q, Renzini A, Le Jeune M, Bayle J-B 2025 LISA GW response Zenodo (https://doi.org/10.5281/zenodo.6423435)
[5] Blanchet L 2002 Gravitational radiation from post-newtonian sources and inspiralling compact binaries *Living Rev. Relativ.* **5** 2
[6] Bressan A, Chiosi C and Fagotto F 1994 Spectrophotometric evolution of elliptical galaxies. I. Ultraviolet excess and color-magnitude-redshift relations *Astrophys. J. Suppl. Ser.* **94** 63
[7] Capetti A, Zamfir S, Rossi P, Bodo G, Zanni C and Massaglia S 2002 On the origin of x-shaped radio-sources: new insights from the properties of their host galaxies *Astron. Astrophys.* **394** 39–45
[8] Caramete L I and Biermann P L 2011 The catalog of nearby black hole candidates (arXiv:1107.2244)
[9] Caramete L I, Balasov R and Păun A 2023 Massive black hole growth using the star gulping mechanism *Rom. Rep. Phys.* **75** 204–204
[10] Caramete L I and Biermann P L 2010 The mass function of nearby black hole candidates *Astron. Astrophys.* **521** A55

[11] Chatziioannou K, Klein A, Yunes N and Cornish N 2017 Constructing gravitational waves from generic spin-precessing compact binary inspirals *Phys. Rev. D* **95** 104004
[12] Cohen M, Wheaton W A and Megeath S T 2003 Spectral irradiance calibration in the infrared. XIV. The absolute calibration of 2MASS *Am. Astron. Soc.* **126** 1090–6
[13] Colpi M et al 2024 Lisa definition study report (arXiv:2402.07571 [astro-ph.CO])
[14] Crain R A *et al* 2015 The eagle simulations of galaxy formation: calibration of subgrid physics and model variations *Mon. Not. R. Astron. Soc.* **450** 1937–61
[15] Dennett-Thorpe J, Scheuer P A G, Laing R A, Bridle A H, Pooley G G and Reich W 2002 Jet reorientation in active galactic nuclei: two winged radio galaxies *Mon. Not. R. Astron. Soc.* **330** 609–20
[16] Feng Y, Di-Matteo T, Croft R A, Bird S, Battaglia N and Wilkins S 2015 The bluetides simulation: first galaxies and reionization *Mon. Not. R. Astron. Soc.* **455** 2778–91
[17] Gergely L A and Biermann P L 2009 The spin-flip phenomenon in supermassive black hole binary mergers *Astrophys. J.* **697** 1621–33
[18] Gergely L A, Biermann P L and Caramete L I 2010 Supermassive black hole spin-flip during the inspiral *Class. Quantum Grav.* **27** 194009
[19] Gopal-Krishna, Biermann P L, Gergely L A and Wiita P J 2012 On the origin of X-shaped radio galaxies *Res. Astron. Astrophys.* **12** 127–46
[20] Hartwig T, Latif M A, Magg M, Bromm V, Klessen R S, Glover S C O, Whalen D J, Pellegrini E W and Volonteri M 2016 Exploring the nature of the Lyman-α emitter CR7 *Mon. Not. R. Astron. Soc.* **462** 2184–202
[21] Hartwig T *et al* 2022 Public release of A-SLOTH: ancient stars and local observables by tracing halos *Astrophys. J.* **936** 45
[22] Henriques B M B, White S D M, Thomas P A, Angulo R, Guo Q, Lemson G, Springel V and Overzier R 2015 Galaxy formation in the Planck cosmology - I. Matching the observed evolution of star formation rates, colours and stellar masses *Mon. Not. R. Astron. Soc.* **451** 2663–80
[23] Hogbom J A and Carlsson I 1974 Observations of the structure and polarization of intense extragalactic sources at 1415 MHz *Astron. Astrophys.* **34** 341–54 (available at: https://ui.adsabs.harvard.edu/abs/1974A%26A....34..341H/abstract)
[24] Husa S, Khan S, Hannam M, Pürrer M, Ohme F, Jiménez Forteza X and Bohé A 2016 Frequency-domain gravitational waves from nonprecessing black-hole binaries. i. new numerical waveforms and anatomy of the signal *Phys. Rev. D* **93** 044006
[25] Into T and Portinari L 2013 New colour-mass-to-light relations: the role of the asymptotic giant branch phase and of interstellar dust *Mon. Not. R. Astron. Soc.* **430** 2715–31
[26] Izquierdo-Villalba D *et al* 2019 J-PLUS: synthetic galaxy catalogues with emission lines for photometric surveys *Astron. Astrophys.* **631** A82
[27] Izquierdo-Villalba D, Sesana A, Bonoli S and Colpi M 2022 Massive black hole evolution models confronting the n-Hz amplitude of the stochastic gravitational wave background *Mon. Not. R. Astron. Soc.* **509** 3488–503
[28] Jarrett T H *et al* 2011 The Spitzer-WISE survey of the ecliptic poles *Astrophys. J.* **735** 112
[29] Katz M L and Larson S L 2019 Evaluating black hole detectability with LISA *Mon. Not. R. Astron. Soc.* **483** 3108–18
[30] Katz M L 2022 Fully automated end-to-end pipeline for massive black hole binary signal extraction from LISA data *Phys. Rev. D* **105** 044055
[31] Katz M L, Marsat S, Chua A J K, Babak S and Larson S L 2020 GPU-accelerated massive black hole binary parameter estimation with LISA *Phys. Rev. D* **102** 023033
[32] Kelly B C and Merloni A 2012 Mass functions of supermassive black holes across cosmic time *Adv. Astron.* **2012** 1–21
[33] Khan S, Husa S, Hannam M, Ohme F, Pürrer M, Forteza X J and Bohé A 2016 Frequency-domain gravitational waves from non-precessing black-hole binaries. ii. a phenomenological model for the advanced detector era *Phys. Rev. D* **93** 044007
[34] Khandai N, Di Matteo T, Croft R, Wilkins S, Feng Y, Tucker E, DeGraf C and Liu M-S 2015 The massiveblack-ii simulation: the evolution of haloes and galaxies to z 0 *Mon. Not. R. Astron. Soc.* **450** 1349–74
[35] Kormendy J and Ho L C 2013 Coevolution (or not) of supermassive black holes and host galaxies *Annu. Rev. Astron. Astrophys.* **51** 511–653
[36] Lagos C P, Tobar R J, Robotham A S G, Obreschkow D, Mitchell P D, Power C and Elahi P J 2018 Shark: introducing an open source, free and flexible semi-analytic model of galaxy formation *Mon. Not. R. Astron. Soc.* **481** 3573–603
[37] Mannerkoski M, Johansson P H, Rantala A, Naab T, Liao S and Rawlings A 2022 Signatures of the many supermassive black hole mergers in a cosmologically forming massive early-type galaxy *Astrophys. J.* **929** 167
[38] McConnell N J and Ma C-P 2013 Revisiting the scaling relations of black hole masses and host galaxy properties *Astrophys. J.* **764** 184
[39] Merritt D and Ekers R D 2002 Tracing black hole mergers through radio lobe morphology *Science* **297** 1310–3
[40] Mezcua M, Lobanov A P, Chavushyan V H and León-Tavares J 2011 Black hole masses and starbursts in x-shaped radio sources *Astron. Astrophys.* **527** A38
[41] Pillepich A *et al* 2017 Simulating galaxy formation with the illustristng model *Mon. Not. R. Astron. Soc.* **473** 4077–106
[42] Pratten G, Klein A, Moore C J, Middleton H, Steinle N, Schmidt P and Vecchio A 2023 Lisa science performance in observations of short-lived signals from massive black hole binary coalescences *Phys. Rev. D* **107** 123026
[43] Pürrer M, Khan S, Ohme F, Birnholtz O and London L 2023 IMRPhenomD: phenomenological waveform model. *Astrophysics Source Code Library, record ascl: 2307.019*
[44] Volonteri M *et al* 2020 Black hole mergers from dwarf to massive galaxies with the newhorizon and horizon-agn simulations *Mon. Not. R. Astron. Soc.* **498** 2219–38
[45] Zier C and Biermann P L 2001 Binary black holes and tori in AGN. I. Ejection of stars and merging of the binary *Astron. Astrophys.* **377** 23–43
[46] Zou F, Brandt W N, Gallo E, Luo B, Ni Q, Xue Y and Yu Z 2024 The cosmic evolution of the supermassive black hole population: a hybrid observed accretion and simulated mergers approach *Astrophys. J.* **976** 6